LISA sources from young massive and open stellar clusters

Sambaran Banerjee[*]

Helmholtz-Instituts für Strahlen- und Kernphysik (HISKP), Nussallee 14-16, D-53115 Bonn, Germany and Argelander-Institut für Astronomie (AIfA), Auf dem Hügel 71, D-53121 Bonn, Germany

(Received 25 June 2020; accepted 28 September 2020; published 2 November 2020)

I study the potential role of young massive star clusters (YMCs) and open star clusters (OCs) in assembling stellar-mass binary black holes (BBHs) which would be detectable as persistent gravitational wave (GW) sources by the forthcoming, space-based Laser Interferometer Space Antenna (LISA). The energetic dynamical interactions inside star clusters make them factories of assembling BBHs and other types of double-compact binaries that undergo general relativistic (GR) inspiraling and merger. The initial phase of such inspirals would, typically, sweep through the LISA GW band. This fabricates a unique opportunity to probe into the early inspiraling phases of merging BBHs, which would provide insights into their formation mechanisms. Here, such LISA sources are studied from a set of evolutionary models of star clusters with masses ranging over $10^4\ M_\odot$–$10^5\ M_\odot$ that represent YMCs and intermediate-aged OCs in metal-rich and metal-poor environments of the local Universe. These models are evolved with long-term, direct, relativistic many-body computations incorporating state-of-the-art stellar evolutionary and remnant formation models. Based on models of the local Universe constructed with such model clusters, it is shown that YMCs and intermediate-aged OCs would yield several tens to hundreds of LISA BBH sources at the current cosmic epoch with GW frequencies within $10^{-3}-10^{-1}$ Hz and signal-to-noise ratios (S/N) > 5, assuming a mission lifetime of 5 or 10 years. Such LISA BBHs would have a bimodal distribution in total mass, be generally eccentric ($\lesssim 0.7$), and typically have similar component masses, although mass-asymmetric systems are possible. Intrinsically, there would be thousands of present-day, LISA-detectable BBHs from YMCs and OCs. That way, YMCs and OCs would provide a significant—in fact, the dominant—contribution to the stellar-mass BBH population detectable by LISA. A small fraction, $< 5\%$, of these BBHs would undergo GR inspiral to make it to LIGO-Virgo GW frequency band and merge within the mission timespan; $< 15\%$ would do so within twice the timespan. LISA BBH source counts for a range of S/N, normalized with respect to the local cluster density, are provided. Drawbacks in the present approach and future improvements are discussed.

DOI: 10.1103/PhysRevD.102.103002

I. INTRODUCTION

Following the recent, above-the-expectation success of the LISA Pathfinder mission [1], the Laser Interferometer Space Antenna (LISA; also, eLISA) has now been approved as an L3 mission by the European Space Agency [2]. LISA is a proposed spaceborne, dual-arm interferometer gravitational wave (hereafter GW) detector with an arm length of 2.5×10^6 km. Such an arm length makes the instrument sensitive to GWs of much lower frequencies, $\sim 10^{-5} - 10^{-1}$ Hz [2], compared to its ground-based counterparts [3,4]. LISA will thus potentially observe a wide variety of low-frequency GW events, such as mergers of binary supermassive black holes, the inspiraling and mergers of binary intermediate-mass black holes, intermediate-mass-ratio and extreme-mass-ratio inspirals involving supermassive and intermediate-mass black holes, Galactic binary white dwarfs and binary stars, and stellar-remnant binary black holes (hereafter BBHs)[1] and other double-compact binaries in the local Universe [2,5–8].

Over their first (O1), second (O2), and third (O3) observing runs, the LIGO-Virgo Collaboration (hereafter LVC) has identified 67 compact binary merger events, which are predominantly BBH merger candidates but also contain binary neutron star (hereafter BNS) and neutron star–black hole (hereafter NSBH) merger events. Among these, the parameter estimations of 11 BBH mergers and 2 BNS mergers have so far been published (see Refs. [9–11], `https://gracedb.ligo.org/superevents/public/O3/`). However, various theories leading to compact binary mergers and their observed properties (see Ref. [12] for a review) still remain largely degenerate.

[*]sambaran@astro.uni-bonn.de; sambaran.banerjee@gmail.com

[1]In this work, "BBH" will imply binary black holes composed of stellar-remnant/stellar-mass black holes.

One of the main reasons for this degeneracy is the fact that most compact binaries "forget" their orbital parameters at formation and hence the imprints of their formation mechanisms, by shrinking to a large extent and becoming practically circular by the time they spiral in, via GW radiation, up to the LIGO-Virgo GW frequency band (∼10–1000 Hz). By probing BBHs and other double-compact binaries at GW frequencies that are lower by a few orders of magnitude, LISA has the potential to identity imprints of such systems' formation mechanisms. In that sense, the identification of BBHs and other double-compact binaries by LISA, and by other proposed decihertz-range space-based GW interferometers such as DECIGO [13,14] and Tian Qin [15,16], would be complementary to the ground-based general relativistic (hereafter GR) merger detections.

In particular, it can generally be expected that BBHs assembled via dynamical interactions in stellar clusters would be eccentric. Dynamically formed BBHs that merge within a Hubble time would exhibit relics of this eccentricity in the LISA frequency band [17,18], on their way to the merger via post-Newtonian (hereafter PN) inspiral. Detailed and self-consistent direct N-body and Monte Carlo simulations of young, open, and globular clusters indeed support this [19–21]. In contrast, isolated binary evolution can be expected to produce predominantly circular BBHs in the LISA band. This is because, in order to place a BBH derived from massive stellar binary evolution in the LISA band, the binary must go through a common envelope (CE) phase [22] so that it shrinks sufficiently [23–27], a process that would also circularize them. Except for the least-massive merging BBHs produced in this way (which would also have the smallest chances of being visible by LISA), which may become eccentric at the beginning of their GR inspiral due to BHs' natal kick [28] (especially that of the later-born BH), the BH members would form via direct collapse without any natal kick, preserving the circular binary orbit.[2]

Note that the typical timescale of PN orbital evolution of BBHs in the LISA band is ∼0.1 Myr, although, depending on the BBH's orbital configuration, it can be as small as ∼10 yr [21]. Therefore, BBHs in the LISA band are persistent or semipersistent GW sources. In contrast, they are transient GW sources in the LIGO-Virgo band, the inspiral timescale being $\lesssim$ a minute.

The contribution of BBH LISA sources from globular clusters (hereafter GCs) and nuclear clusters (hereafter NSCs) in the local Universe, due to dynamical processes in such clusters, has recently been studied [20,31,32]. This study investigates BBH LISA sources from young massive clusters (hereafter YMCs) and open clusters (hereafter OCs), an aspect which is rather unexplored to date. To that end, the set of theoretical cluster evolutionary models as described in Ref. [21] is utilized. The structure and stellar composition of these cluster models are consistent with those observed in YMCs and OCs in the Milky Way and the Local Group. The models are evolved with state-of-the-art PN direct N-body integration, incorporating up-to-date supernova (hereafter SN) and stellar remnant formation models.

In Sec. II A, the N-body evolutionary models of star clusters and BBH inspirals from them are summarized. Section II B discusses the method of constructing models of the local Universe with these cluster models and obtaining present-day LISA BBH sources from them. Section III estimates the LISA BBH source counts and the sources' properties. Section IV summarizes and discusses the present results and their caveats, and suggests upcoming improvements.

II. COMPUTATIONS

In this section, the approach to determining the LISA source count and properties, based on model cluster evolution, is described.

A. Post-Newtonian, many-body cluster evolutionary models

In this work, the 65 N-body evolutionary models of star clusters, as described in Ref. [21], are utilized. The model clusters initially possess a Plummer density profile [33] for the spatial distribution of all constituent stars, are in virial equilibrium [34,35], have masses $10^4\ M_\odot \leq M_{cl}(0) \leq 10^5\ M_\odot$, and have half-mass radii $1\ \mathrm{pc} \leq r_h(0) \leq 3\ \mathrm{pc}$. They range over $0.0001 \leq Z \leq 0.02$ in metallicity and are subjected to a solar-neighborhood-like external galactic field. The initial models are composed of zero-age main sequence (hereafter ZAMS) stars with masses over $0.08\ M_\odot$–$150.0\ M_\odot$ and distributed according to the standard initial mass function (hereafter IMF). About half of these models have a primordial binary population (overall initial binary fraction ≈5% or 10%), where all the O-type stars (i.e., stars with ZAMS mass down to $16\ M_\odot$) are paired among themselves with an observationally motivated distribution of massive stellar binaries [36,37]. Although idealistic, such cluster parameters and stellar compositions are consistent with those observed in YMCs and medium-mass OCs that continue to form and dissolve in the Milky Way and other Local Group galaxies.

These model clusters are evolved using NBODY7, a state-of-the-art PN direct N-body integrator [38–40] that couples with the semianalytical (or population synthesis) stellar and binary evolutionary model BSE [41,42]. The integrated BSE is made up to date [28] in regard to prescriptions of stellar

[2]If the natal kick of stellar remnants is predominantly due to asymmetric emission of neutrinos [29,30], then direct collapse BHs would also receive significant natal kicks [28]. In that case, finding out how orbital characteristics of field BBHs in the LISA band would compare with dynamically assembled BBHs requires detailed modeling of a neutrino-driven kick in a population synthesis of massive binaries.

wind mass loss [43] and the formation of stellar-remnant neutron stars (hereafter NSs) and black holes (hereafter BHs) by incorporating the "rapid" and "delayed" SN models [44] and pulsation pair-instability (PPSN) and pair-instability (PSN) supernovae [45]. The SN remnants receive natal velocity kicks that are scaled down from a Maxwellian distribution with dispersion equal to the velocity dispersion of single NSs in the galactic field ($\approx 265\ \mathrm{km\,s^{-1}}$) [46]. The scaledown is applied based on material fallback onto the protoremnant in the SN [44] and according to the conservation of linear momentum (popularly referred to as the "momentum-conserving natal kick" [26,47]). This slowdown procedure allows the natal kicks of $\gtrsim 10\ M_\odot$ BHs [28] to be less than the parent clusters' escape speeds; such BHs are, therefore, retained back into the clusters right after their birth.

The PN treatment of NBODY7 is handled by an ARCHAIN sub-integrator [48,49] that applies PN corrections (up to PN-3.5) to a binary with a NS or a BH component that either is by itself gravitationally bound to the cluster or is a part of an in-cluster triple or higher-order subsystem. The (regularized) PN orbital integration of the binary takes into account perturbations from the outer members (if part of a subsystem) until the subsystem is resolved, via either the binary's GR inspiral and coalescence or the disintegration of the subsystem. This allows in-cluster GR mergers driven by the Kozai-Lidov (hereafter KL) mechanism [50–52] or chaotic triple (or higher-order) interactions (e.g., Refs. [31,53]). Apart from such in-cluster mergers, which compose the majority of the GR mergers from these model clusters, a fraction of the double-compact binaries ejected dynamically from the clusters would also undergo PN inspiraling and merger within a Hubble time (e.g., Refs. [54–58]). As demonstrated in Refs. [19,21] (see also Ref. [20]), the vast majority of such in-cluster and ejected dynamically driven inspirals, most of which are BBH inspirals, initiate with a peak GW frequency lying within or below the LISA band. Although most of these inspirals begin with very high eccentricity, they circularize via GR inspiraling [59] to become moderately eccentric ($\lesssim 0.7$) within the LISA band, and would be visible by the instrument [17,18,60].

The stellar remnant BHs are assigned spins at birth based on hydrodynamic models of fast-rotating massive single stars [61], which are utilized in assigning numerical-relativity-based GR merger recoil kicks and final spins [62–64] of the in-cluster BBH mergers. However, the ARCHAIN PN integrations are themselves performed assuming nonspinning members for ease of computing; this simplification is not critical for LISA GW frequencies, since spin-orbit precession and the corresponding modification of orbital evolutionary time would be mild over such frequencies. In the computed models of Ref. [21], the majority of the BBH mergers have primaries $\mathrm{M}_1 \lesssim 40\ M_\odot$. Rarely, M_1 reaches up to $\approx 100\ M_\odot$ (total mass up to $\approx 140\ M_\odot$) due to the occurrence of second-generation BBH mergers [65,66] or BBH mergers involving a BH that has previously gained mass via merging with a regular star (forming a BH Thorne-Zytkow object) [21]. Further details of these computed star cluster models are given in Ref. [21], and the stellar and binary evolutionary schemes used in these models are further elaborated in Ref. [28].

Note that the present cluster models initiate with a Plummer density profile in virial equilibrium. However, the initial density profile is unlikely to significantly influence the GR inspiral events (their number, rate, and properties) from the clusters. This is because the dynamically triggered GR inspirals take place due to the close encounters in the "BH core," which is formed after the BHs (that are retained in the cluster after their birth; see above) segregate in the innermost region of the cluster [55,67], in ~ 100 Myr for the masses and sizes of the present models [34]. The properties of this BH core (or BH subcluster), and hence those of the BBHs formed inside it, depend mostly on the bulk properties of the whole star cluster, such as its mass and virial radius [68–70]. Note further that, in reality, the (proto)clusters would initially have been subvirial and contained substructures—or, alternatively, would have gone through a supervirial phase due to residual gas expulsion, as suggested by observations of molecular clouds, young stellar nurseries, and young clusters [71–73]. However, as long as a cluster survives such an initial "violent relaxation" phase (so that it becomes a "fully formed cluster" as modeled here; see also Sec. IV), the substructures would be washed out and the cluster would become (near) spherical and virialized in a few dynamical (or free-fall) times, typically in ~Myr [74–78]—i.e., much earlier than the "BH core" formation.

The initially $\approx 100\%$ primordial binary fraction among the BH-progenitor O-type stars (see above) moderately affects, through binary evolution [21,28,58,79], the mass distribution of the BHs retained in the clusters. However, since inside a dynamically active BH core (i.e., a core that is efficiently producing BBHs and their inspiral mergers through dynamical interactions) the BHs interact mostly among themselves and rarely with the regular stars and their binaries [80–82], the primordial binary fraction among the lower-mass stars ($\approx 5\%$ or 10% in the present models; see above) is unlikely to largely influence the BBH production (the dynamical heating from the stellar binaries may mildly affect the structure of the cluster, and hence that of the BH subsystem). In some computed clusters, an alternative, the "collapse-asymmetry-driven" natal kick model [83–86], is applied instead of the standard momentum-conserving kick (see above). The collapse-asymmetry-driven kick model, in addition to incorporating slowdown due to SN material fallback, applies additional slowing down mechanism (with recipes based on numerical computations of stellar collapse) for NSs and low-mass BHs ($\lesssim 10\ M_\odot$) arising from the washing out of asymmetries in

the pre-SN star due to convection; see Ref. [28] and references therein for further detail. Since young and open clusters, which are of age $\lesssim$Gyr, are considered here (see Sec. II B), the least massive BHs would mostly be dynamically inert over the clusters' age range (e.g., Ref. [87]). Therefore, the use of this alternative natal kick recipe in a few models is unlikely to have a substantial influence on the overall BBH/inspiral-merger yield from these models.

In summary, current specifics of the initial cluster models or their potential alternatives (e.g., the use of initially King or fractal profiles instead of Plummer, higher primordial binary fractions among non-BH-progenitor stars) would, at best, have an order-unity influence on the BBH production and their GR inspiral and merger events from the models. The initial mass and size ranges considered in these modes are consistent with those observed for young massive clusters in the local Universe [88]. Alternative model ingredients will be explored in a future study.

B. Present-day LISA sources from computed cluster models

A "sample local Universe" is constructed out of N_{samp} model clusters by placing each cluster at a random comoving distance, D, within a spherical volume of $D_{max} = 1500$ Mpc, centered around the detector. The value of D_{max} is set based on the fact that at this distance the brightest LISA sources from the computed models still project characteristic strain marginally above LISA's design noise floor (see below). In other words, D_{max} is the limit of visibility of BBH sources, as of the present computed models.

For each cluster at a chosen distance D, a model of mass, $M_{cl}(0)$, is selected from the set of computed cluster models, with probability $\propto M_{cl}(0)^{-2}$ over its range of $10^4\ M_\odot$–$10^5\ M_\odot$ in the set. Such a mass distribution is observed for newborn and young clusters of a wide mass range in the Milky Way and nearby galaxies [89–92]. The model's size is selected uniformly over its range in the computed set—i.e., $1\ \mathrm{pc} \le r_h(0) \le 3\ \mathrm{pc}$, and its metallicity is chosen uniformly over $Z_{min} \le Z \le Z_{max}$. Two metallicity ranges are considered: that of the entire model set, $(Z_{min}, Z_{max}) = (0.0001, 0.02)$, ranging from very metal-poor environments up to the solar enrichment, and $(Z_{min}, Z_{max}) = (0.005, 0.02)$, comprising only metal-rich systems (down to $0.25Z_\odot$). Note that most of the models in the wider Z range case have $Z \ge 0.001$ (see Ref. [21]) as consistent with the most metal-poor galaxies observed in the local Universe [93]. The choice of two Z ranges allows studying the impact of metallicity on LISA source counts and properties. As shown in Table I, local Universe samples of $N_{samp} \sim 10^4$ are considered, a sample size that provides a fair balance between the computing time required for extracting the present-day LISA sources (see below) and statistics.

Each cluster in a sample is assigned a formation redshift, z_f, that corresponds to an age, t_f, of the Universe. A GR inspiral in the LISA frequency band occurs from this cluster (the vast majority of the inspirals are of BBHs; see Ref. [21]) after a delay time, t_{delay}, from the formation, when the age of the Universe is t_{event}—i.e.,

$$t_{event} = t_f + t_{delay}. \tag{1}$$

If the light travel time from the cluster's distance, D, is t_{lD}, then the age of the Universe is

$$t_{obs} = t_{event} + t_{lD} \tag{2}$$

when the (redshifted) GW signal reaches the detector. The formation epoch, z_f, of a cluster is assigned according to the probability distribution given by the cosmic star formation history (hereafter SFH), namely [94]

$$\psi(z) = 0.015 \frac{(1+z)^{2.7}}{1+[(1+z)/2.9]^{5.6}}\ M_\odot\ \mathrm{yr}^{-1}\ \mathrm{Mpc}^{-3}. \tag{3}$$

A detected signal is considered "recent" if

$$t_{Hubble} - \Delta t_{obs} \le t_{obs} \le t_{Hubble} + \Delta t_{obs}, \tag{4}$$

TABLE I. LISA source counts based on representative samples of the local Universe ($D \le 1500$ Mpc), as constructed with the computed model clusters (Secs. II A and II B). Col. 1: metallicity (Z) range of the model clusters in a sample. Col. 2: lifetime of the LISA mission, T_{LISA}. Col. 3: number of clusters, N_{samp}, in the sample. Col. 4: intrinsic number of LISA sources, N_0, at the present cosmic age (within $t_{Hubble} \pm 0.1$ Gyr) from the sample. Col. 5: inferred intrinsic number of LISA sources within T_{LISA}, $\mathcal{N}_0$, scaled by the cluster density (in Mpc^{-3}) of the local Universe, ρ_{cl}. Cols. 6, 8, 10: numbers of LISA sources from the sample, $N_{>2}$, $N_{>5}$, and $N_{>10}$, with S/N ≥ 2, ≥ 5, and ≥ 10, respectively, at the present cosmic age. Cols. 7, 9, 11: inferred numbers of LISA sources within T_{LISA}, $\mathcal{N}_{>2}$, $\mathcal{N}_{>5}$, and $\mathcal{N}_{>10}$, with S/N ≥ 2, ≥ 5, and ≥ 10, respectively, scaled by the cluster density of the local Universe [Eq. (27)].

Z	T_{LISA}/yr	N_{samp}	N_0	$\mathcal{N}_0/\rho_{cl}$	$N_{>2}$	$\mathcal{N}_{>2}/\rho_{cl}$	$N_{>5}$	$\mathcal{N}_{>5}/\rho_{cl}$	$N_{>10}$	$\mathcal{N}_{>10}/\rho_{cl}$
0.0001–0.02	5.0	23508	1329	19.98	222	3.34	72	1.08	39	0.59
0.005–0.02	5.0	23172	917	13.99	135	2.06	56	0.85	29	0.44
0.0001–0.02	10.0	23364	1276	38.61	307	9.29	104	3.15	45	1.36
0.005–0.02	10.0	22896	924	28.53	157	4.85	53	1.64	30	0.93

where $t_{\rm Hubble}$ is the present age of the Universe (the Hubble time) and $\Delta t_{\rm obs}$ is taken to be $\Delta t_{\rm obs} = 0.1$ Gyr. $\Delta t_{\rm obs}$ serves as an uncertainty in the cluster formation epoch; with the above choice it is well within the typical epoch uncertainties in the observed SFH data [94]. In this work, the contributions of LISA sources from young and open clusters are considered, which is why the formation epoch is restricted to relatively recent times—namely, $0.0 \leq z_{\rm f} \leq 0.5$—that correspond to formation lookback times within 0.0 Gyr $\leq t_{{\rm lb},f} \lesssim 5$ Gyr.

The peak power GW frequency in the source frame, $f_{\rm GWp}$, from a GR inspiraling binary of component masses $(\mathrm{M}_1, \mathrm{M}_2)$ and with instantaneous semimajor axis a and eccentricity e is given by [95]

$$f_{\rm GWp} = \frac{\sqrt{G(\mathrm{M}_1+\mathrm{M}_2)}}{\pi}\frac{(1+e)^{1.1954}}{[a(1-e^2)]^{1.5}}. \tag{5}$$

The orbital parameters (a, e) decay due to the orbit-averaged leading gravitational radiation (PN-2.5 term) as (in the source frame) [59]

$$\left.\begin{aligned}\dot{a} &= -\tfrac{64}{5}\frac{G^3\mathrm{M}_1\mathrm{M}_2(\mathrm{M}_1+\mathrm{M}_2)}{c^5a^3(1-e^2)^{7/2}}\left(1+\tfrac{73}{24}e^2+\tfrac{37}{96}e^4\right)\\ \dot{e} &= -\tfrac{304}{15}\frac{G^3\mathrm{M}_1\mathrm{M}_2(\mathrm{M}_1+\mathrm{M}_2)}{c^5a^4(1-e^2)^{5/2}}e\left(1+\tfrac{121}{304}e^2\right)\end{aligned}\right\}. \tag{6}$$

Note that $f_{\rm GWp}$ is a certain harmonic, n_p, of the Keplerian orbital frequency, $f_{\rm K}(=1/2\pi\sqrt{G(\mathrm{M}_1+\mathrm{M}_2)/a^3})$, i.e.,

$$f_{\rm GWp} = n_p f_{\rm K}. \tag{7}$$

Hence, n_p decreases with the binary's orbital evolution (i.e., with decreasing e), such that $n_p \lesssim 10$ for $e \lesssim 0.7$ and $n_p = 2$ for $e = 0$. For low GW frequencies, the frequency time derivative or "chirp" is given by

$$\dot{f}_{\rm GWp} \approx n_p\dot{f}_{\rm K} = n_p\frac{48}{5\pi}\frac{(GM_{\rm ch})^{5/3}}{c^5}(2\pi f_{\rm K})^{11/3}F(e), \tag{8}$$

which can be obtained by utilizing the expression of $\dot{a}$ from Eq. (6) (see, e.g., Ref. [20]). Here $M_{\rm ch} \equiv (\mathrm{M}_1\mathrm{M}_2)^{3/5}/(\mathrm{M}_1+\mathrm{M}_2)^{1/5}$ is the source-frame chirp mass, and

$$F(e) \equiv \frac{1}{(1-e^2)^{7/2}}\left(1+\frac{73}{24}e^2+\frac{37}{96}e^4\right) \tag{9}$$

is the "eccentricity correction factor" of Eq. (6).

At the peak frequency and from distance D, the characteristic strain (including inclination averaging; see, e.g., Refs. [20,96]), $\tilde{h}_c$, of the GW is given by [20,96,97]

$$\tilde{h}_c^2 = \frac{2}{3\pi^{4/3}}\frac{G^{5/3}}{c^3}\frac{M_{\rm ch}^{5/3}}{D^2}\frac{1}{f_{\rm GWp}^{1/3}}\left(\frac{2}{n_p}\right)^{2/3}\frac{g(n_p,e)}{F(e)}, \tag{10}$$

where $g(n,e)$ is the relative GW power function as given by [96]

$$g(n,e) = \frac{n^4}{32}\left\{\left[J_{n-2}(ne) - 2eJ_{n-1}(ne) + \frac{2}{n}J_n(ne) + 2eJ_{n+1}(ne) - J_{n+2}(ne)\right]^2 + (1-e^2)[J_{n-2}(ne) - 2J_n(ne) + J_{n+2}(ne)]^2 + \frac{4}{3n^2}[J_n(ne)]^2\right\}. \tag{11}$$

J_n is the Bessel function of order n [98].

Equation (10) can be obtained by combining the general expression for GW characteristic strain, $\tilde{h}_{c,n}$, for the nth harmonic with the source-frame frequency $f'_n = nf_{\rm K}$, as given by (e.g., Ref. [97])

$$\tilde{h}_{c,n}^2 = \frac{1}{(\pi D)^2}\left(\frac{2G}{c^3}\frac{P_n}{\dot{f}'_n}\right) \tag{12}$$

with the average GW power, P_n, emitted by the source at the nth harmonic as given by [96]

$$P_n = \frac{32}{5}\frac{G^4}{c^5}\frac{\mathrm{M}_1^2\mathrm{M}_2^2(\mathrm{M}_1+\mathrm{M}_2)}{a^5}g(n,e). \tag{13}$$

Using the facts that $\dot{f}'_n \approx n\dot{f}_{\rm K}$ analogously to Eq. (8) and that $f_{\rm K} = 1/2\pi\sqrt{G(\mathrm{M}_1+\mathrm{M}_2)/a^3}$ (e.g., Ref. [20]),

$$\tilde{h}_{c,n}^2 = \frac{2}{3\pi^{4/3}}\frac{G^{5/3}}{c^3}\frac{M_{\rm ch}^{5/3}}{D^2}\frac{1}{f_n'^{1/3}}\left(\frac{2}{n}\right)^{2/3}\frac{g(n,e)}{F(e)}, \tag{14}$$

which becomes Eq. (10) by substituting $f'_n = f_{\rm GWp}$ and $n = n_p$.

If the redshift at the cluster's distance is $z_{\rm D}$, then the detector-frame (redshifted) peak GW frequency, its chirp, and the chirp mass are given by

$$\left.\begin{aligned}f_{\rm GWp,z} &= \tfrac{f_{\rm GWp}}{(1+z_{\rm D})}\\ \dot{f}_{\rm GWp,z} &= \tfrac{\dot{f}_{\rm GWp}}{(1+z_{\rm D})^2}\\ M_{\rm ch,z} &= M_{\rm ch}(1+z_{\rm D})\end{aligned}\right\}. \tag{15}$$

The detector-frame chirp mass can be obtained by rewriting Eq. (8) in terms of $f_{\rm GWp,z}$, and $\dot{f}_{\rm GWp,z}$.

In this work, a GW source is considered visible by LISA if (i) its GW frequency lies within a relatively narrow range, 10^{-3} Hz $\leq f_{\rm GWp,z} \leq 10^{-1}$ Hz, around the instrument's noise floor minimum or "bucket frequency" (at $\sim 10^{-2}$ Hz; see Refs. [2,99]). At the same time, (ii) a LISA-visible source should at most be moderately eccentric, $e \leq 0.7$ [17,18,60], so that it is not "bursty." Note that a source is effectively less detectable the slower the evolution of $f_{\rm GWp,z}$ ($f_{\rm GWp}$) is over the LISA mission lifetime, $T_{\rm LISA}$. This is taken into account by multiplying by a reduction factor to the GW characteristic strain, as given by Eq. (10):

$$h_c = \kappa \times \tilde{h}_c, \tag{16}$$

where [20,100,101]

$$\kappa = \min\left(\sqrt{\frac{\dot{f}_{\rm GWp,z}}{f_{\rm GWp,z}} T_{\rm LISA}}, 1\right). \tag{17}$$

Here, mission lifetimes of $T_{\rm LISA} = 5$ yr (planned) and 10 yr (optimistic) are considered.

Finally, (iii) h_c should exceed a signal-to-noise ratio (hereafter S/N) threshold for visibility. In this work, LISA sources with S/N > 0, ≥ 2, ≥ 5, and ≥ 10 are considered; the source count with S/N > 0 implies the intrinsic count. The analytical LISA design sensitivity curve (or noise floor) [99], which closely reproduces the instrument's published design sensitivity curve [2] over the visibility frequency window considered here, is utilized in determining the S/N for the LISA sources from the sample Local Universe. In terms of characteristic strain, this sensitivity curve as a function of (detector-frame) GW frequency, f, is given by

$$\left.\begin{aligned} h_{\mathcal{N}}(f) &= f^{1/2}\sqrt{S_{\mathcal{N}}(f) + S_{\rm g}(f)} \\ S_{\mathcal{N}}(f) &= \tfrac{P_{\mathcal{N}}(f)}{\mathcal{R}(f)} \end{aligned}\right\}. \tag{18}$$

Here, $P_{\mathcal{N}}(f)$ is the power spectral density of the (LISA) instrument noise, and $\mathcal{R}(f)$ is the sky- and polarization-averaged, two-channel (since LISA has two independent data channels) signal response function. The added $S_g(f)$ is the power spectral density (divided by 2 due to the two-channel instrument) of the confusion noise due to unresolved Galactic binaries.

With the analytic fit to the response function, as given by

$$\mathcal{R}(f) = \frac{3}{10}\frac{1}{(1 + 0.6(f/f_*)^2)}, \tag{19}$$

$$S_{\mathcal{N}}(f) = \frac{10}{3L^2}\left(P_{\rm OMS}(f) + 2(1 + \cos^2(f/f_*))\frac{P_{\rm acc}(f)}{(2\pi f)^4}\right) \times \left(1 + \frac{6}{10}\left(\frac{f}{f_*}\right)^2\right). \tag{20}$$

The functions $P_{\rm OMS}(f)$ (single-link optical metrology noise) and $P_{\rm acc}(f)$ (single-test-mass acceleration noise) are given by (as in "LISA Strain Curves" Report No. LISA-LCST-SGS-TN-001)

$$\left.\begin{aligned} P_{\rm OMS}(f) &= (1.5 \times 10^{-11}\ {\rm m})^2\left(1 + \left(\tfrac{2\ {\rm mHz}}{f}\right)^4\right)\ {\rm Hz}^{-1} \\ P_{\rm acc}(f) &= (3 \times 10^{-15}\ {\rm m\,s^{-2}})^2\left(1 + \left(\tfrac{0.4\ {\rm mHz}}{f}\right)^2\right) \\ &\quad \times\left(1 + \left(\tfrac{f}{8\ {\rm mHz}}\right)^4\right)\ {\rm Hz}^{-1} \end{aligned}\right\}, \tag{21}$$

and the instrument constants are $L = 2.5$ Gm (LISA arm length) and $f_* = 19.09$ mHz. The Galactic confusion noise is given by the fitting function

$$S_g(f) = A f^{-7/3} e^{-f^\alpha + \beta f \sin(Kf)}[1 + \tanh(\gamma(f_k - f))]\ {\rm Hz}^{-1} \tag{22}$$

with $A = 9 \times 10^{-45}$, $\alpha = 0.138$, $\beta = -221$, $K = 521$, $\gamma = 1680$, and $f_k = 0.00113$. See Ref. [99] and references therein for the derivations of Eqs. (19), (20), (21), and (22).

The resulting LISA design sensitivity curve is shown in the panels of Fig. 1 (thick blue line). Note that f_k and γ in Eq. (22) vary moderately with observation time, resulting in an increasingly steep dropoff of $S_{\rm g}(f)$. Here, for simplicity, the four-year values of all the parameters in Eq. (22), as stated above [99], are used. Note that over most of the LISA detection frequency range, $S_{\mathcal{N}}$ is the dominant noise, except that $S_{\rm g}$ causes the mild "hump" feature in the total sensitivity curve, as seen in Fig. 1.

In this work, for simplicity, S/N is preliminarily taken to be [recalling Eq. (16)]

$$\left(\frac{\rm S}{\rm N}\right) \approx \frac{h_c(f_{\rm GWp})}{h_{\mathcal{N}}(f_{\rm GWp,z})} = \frac{\kappa(f_{\rm GWp,z})\tilde{h}_c(f_{\rm GWp})}{h_{\mathcal{N}}(f_{\rm GWp,z})} \tag{23}$$

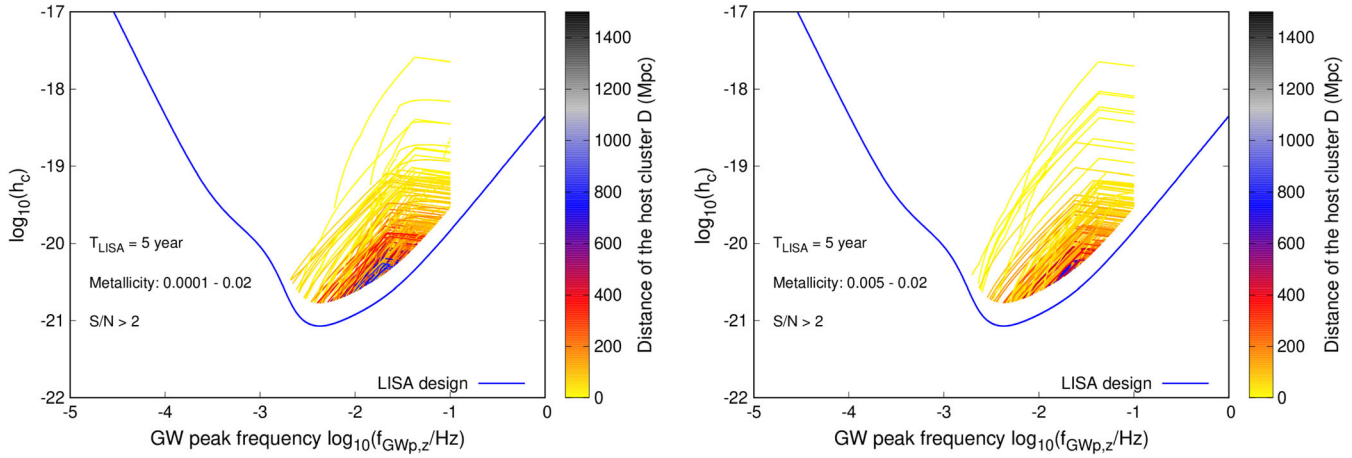

FIG. 1. BBH inspirals at the present cosmic age (within $t_{\rm Hubble} \pm 0.1$ Gyr), over the characteristic LISA frequency range ($10^{-3} - 10^{-1}$ Hz), from a representative sample of the local Universe ($D \leq 1500$ Mpc) as constructed with the computed model clusters (Sec. II). The inspirals are shown (thin lines) in the plane of redshifted GW peak frequency in the detector frame, $f_{\rm GWp,z}$, versus GW characteristic strain at this frequency, h_c, for those systems which have S/N ≥ 2 with respect to LISA's design sensitivity curve (thick blue line). The $h_c - f_{\rm GWp,z}$ tracks are color coded (color bar) according to the distance of the BBH's host cluster. The left and right panels show the outcomes when the metallicity range of the model clusters in the local Universe sample is taken to be 0.0001–0.02 and 0.005–0.02, respectively. A LISA mission lifetime of $T_{\rm LISA} = 5$ yr is assumed.

$[f_{\rm GWp} = (1+z_{\rm D}) f_{\rm GWp,z}]$, which is evaluated along an inspiraling orbit using Eqs. (5), (6), (10), (17), and (18)–(22). [In the practical computations, a lookup table for the LISA design noise strains, generated using Eqs. (20)–(22), is utilized.] A more elaborate expression of S/N is given by summing over all harmonics [102][3]:

$$\left(\frac{\rm S}{\rm N}\right) = \sqrt{\sum_{n=1}^{\infty} \int_{f_{n,0}}^{f_{n,T_{\rm LISA}}} \left[\frac{\tilde{h}_{c,n}(f'_n)}{h_{\mathcal{N}}(f_n)}\right]^2 d\ln f_n} \qquad (24)$$

$[f'_n = (1+z_{\rm D}) f_n]$. Here, f_n is the detector-frame GW frequency of the nth harmonic (see above), and $(f_{n,0}, f_{n,T_{\rm LISA}})$ is the GW frequency of this harmonic at the (start, end) of LISA observation at time $(0, T_{\rm LISA})$. $\tilde{h}_{c,n}(f'_n)$ is the GW characteristic strain corresponding to the nth harmonic as given by Eq. (14).

Since the majority of the LISA-visible binaries have mild eccentricity [due to condition (ii) and also GR orbital evolution; see below], the GW power is sharply peaked at the peak GW frequency $f_{\rm GWp}$ ($f_{\rm GWp,z}$) [96], which corresponds to the harmonic $n_p \lesssim 10$ (see above). In that case, Eq. (24) becomes, to the leading order,

$$\left(\frac{\rm S}{\rm N}\right) \approx \sqrt{\int_0^{T_{\rm LISA}} \left[\frac{\tilde{h}_c(f_{\rm GWp})}{h_{\mathcal{N}}(f_{\rm GWp,z})}\right]^2 \frac{\dot{f}_{\rm GWp,z}}{f_{\rm GWp,z}} dt}$$
$$\approx \sqrt{\left[\frac{\tilde{h}_c(f_{\rm GWp})}{h_{\mathcal{N}}(f_{\rm GWp,z})}\right]^2 \frac{\dot{f}_{\rm GWp,z}}{f_{\rm GWp,z}} T_{\rm LISA}}$$
$$= \frac{\kappa(f_{\rm GWp,z}) \tilde{h}_c(f_{\rm GWp})}{h_{\mathcal{N}}(f_{\rm GWp,z})} \qquad (25)$$

$[f_{\rm GWp} = (1+z_{\rm D}) f_{\rm GWp,z}]$, where the last equality is due to Eq. (17). In the second approximate relation in Eq. (25), the integrand, to its leading order, is taken to remain constant at its mean value over $T_{\rm LISA}$, since its variation over $T_{\rm LISA}$ is typically small ($\kappa < 1$ for most sources here; see Fig. 3 and the associated discussions below). Therefore, the approximate S/N, as given by Eq. (23), serves as a good approximation for and captures the essential properties of the full definition, for the LISA sources in this work.[4]

[3]Alternatively, $\tilde{h}_c$ and $\tilde{h}_{c,n}$ can also be expressed in terms of quantities in the detector frame using Eq. (15) (as, e.g., in Ref. [20]). Since here, the source-frame quantities are available directly from the computed models, it is natural to express $\tilde{h}_c$ and $\tilde{h}_{c,n}$ in terms of source-frame GW frequency and chirp mass, and to redshift these quantities to the detector frame [Eq. (15)].

[4]If, in the presently considered LISA frequency range [condition (i)], $f_{\rm GWp,z}/\dot{f}_{\rm GWp,z} < T_{\rm LISA}$ (i.e., $\kappa = 1$), then the integral in Eq. (25) can be subdivided over intervals of $\Delta T < T_{\rm LISA}$ such that $(\dot{f}_{\rm GWp,z}\Delta T)/f_{\rm GWp,z} \sim 1$, and the same approximation can be applied over each subintegral, still being consistent with Eq. (23). With the approximate S/N evaluated here, marginal sources, whose nondominant harmonics would add up to exceed the S/N threshold, are missed, and consequently, the present source counts serve as lower limits. However, the underestimation would be to a small extent, since, for the present sources, the GW power spectrum is sharply peaked at $f_{\rm GWp}$ due to the sources' mild/small eccentricity (see text). Similarly, weak but transient (with respect to $T_{\rm LISA}$; i.e., $\kappa = 1$) sources, whose S/N would integrate up over $T_{\rm LISA}$, are also missed. Such underestimation would also be small, since nearly all sources here enter the considered LISA frequency range with $\kappa_1 < 1$ (see Fig. 3 and the associated discussions in the text).

The squared value of κ [Eq. (17)] at the minimum $f_{\mathrm{GWp,z}}$ for which the visibility conditions (i), (ii), and (iii) are simultaneously satisfied (i.e., at the source's "entry" to the visibility band) is referred to in this work as the "transience," κ_1, of the LISA source. $\kappa_1 \leq 1$ is a measure of how transient the source is over the LISA lifetime: the larger the value of κ_1, the more the source's $f_{\mathrm{GWp,z}}$ and other properties will evolve (due to its PN inspiral) over the mission lifetime. $\kappa_1 = 1$ implies that the source evolves in a timescale $\leq T_{\mathrm{LISA}}$.

In this study, the standard (ΛCDM) cosmological framework is adopted [103] with the cosmological constants from the latest Planck results (H_0=67.4kms^{-1}Mpc^{-1}, Ω_m=0.315, and a flat Universe for which $t_{\mathrm{Hubble}} = 13.79$ Gyr) [104].

III. LISA SOURCES FROM YOUNG MASSIVE AND OPEN STELLAR CLUSTERS

Figure 1 shows examples of BBH inspirals in the LISA band from a sample local Universe that are "detected" [i.e., they satisfy the visibility conditions (i)–(iii)] at the present cosmic age with $\mathrm{S/N} \geq 2$ (i.e., at $|t_{\mathrm{obs}} - t_{\mathrm{Hubble}}| \leq \Delta t_{\mathrm{obs}} [= 0.1\ \mathrm{Gyr}]$), using the method described in Sec. II B. Figure 1 shows the detected inspirals [as dictated by Eqs. (6), (10), and (17)] in the $h_c - f_{\mathrm{GWp,z}}$ plane for the Z ranges 0.0001–0.02 and 0.005–0.02, and for $T_{\mathrm{LISA}} = 5$ yr (see Table I). The design sensitivity curve of LISA [99] is shown in the same plane (the thick blue line). In the following, unless otherwise stated, present-day (or present-cosmic-age) LISA sources will imply only those that are detected in the above sense. Note that depending on the strength of a particular source (given its distance, mass, and orbital properties), it may be detectable over only a subwindow within the full detection frequency range $10^{-3} - 10^{-1}$ Hz (see Fig. 1).

If, for the T_{LISA} mission time, the total number of present-day LISA sources with $\mathrm{S/N} \geq s$ from a sample local Universe comprising $\mathrm{N_{samp}}$ clusters is $\mathrm{N}_{>s}$, then the estimated number of present-day LISA sources within a T_{LISA} window, $\mathcal{N}_{>s}$, is

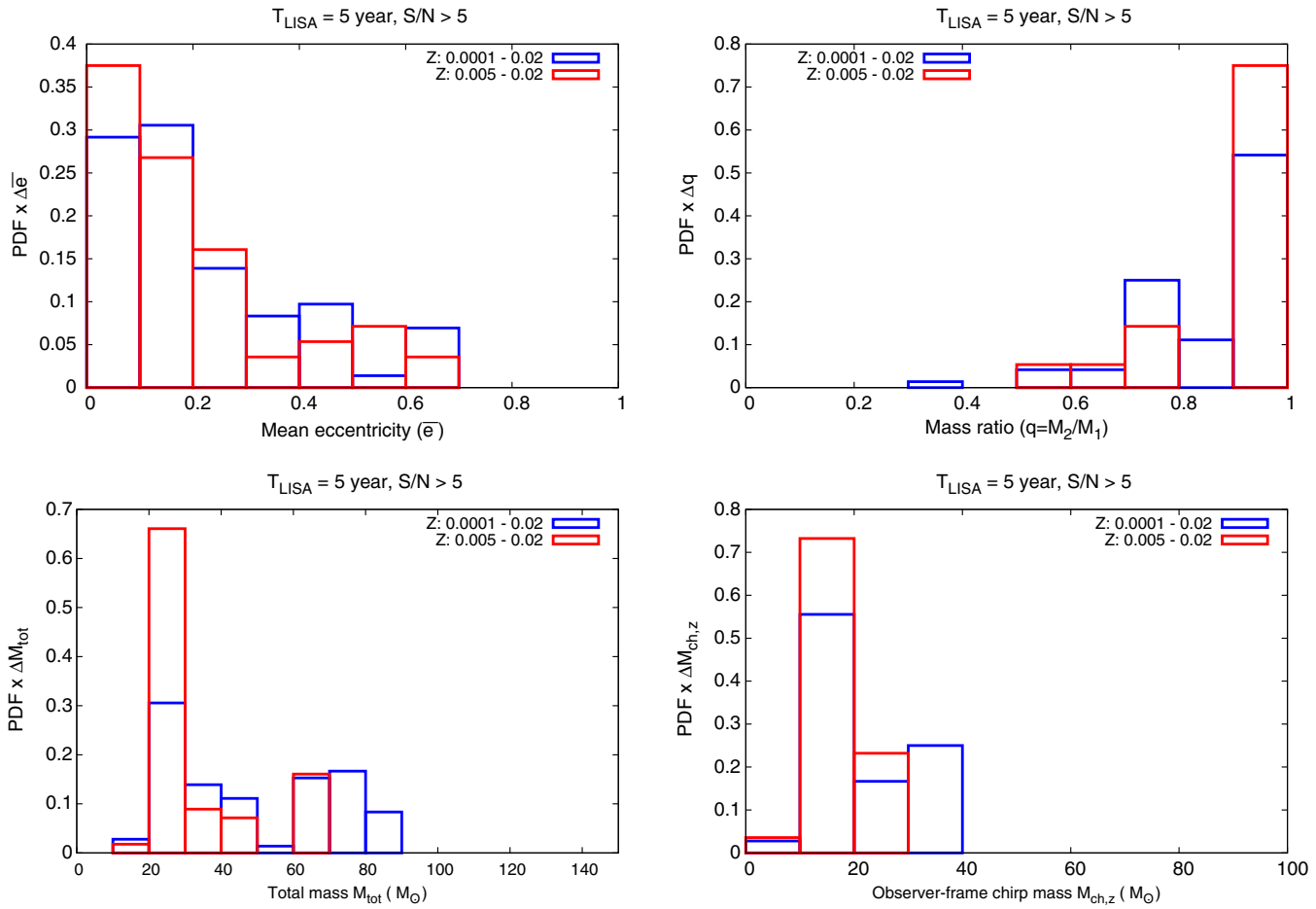

FIG. 2. Properties of LISA BBH sources, with $\mathrm{S/N} > 5$, at the present cosmic age from a representative local Universe constructed with the computed model clusters (Sec. II). The top-left, top-right, bottom-left, and bottom-right panels show the probability distributions of the sources' mean eccentricity (Sec. III) $\bar{e}$, the mass ratio q, the total mass M_{tot}, and the detector-frame (redshifted) chirp mass $M_{\mathrm{ch,z}}$, respectively. In each panel, the blue- and red-lined histograms correspond to the cluster metallicity ranges 0.0001–0.02 and 0.005–0.02, respectively. A LISA mission lifetime of $T_{\mathrm{LISA}} = 5$ yr is assumed.

$$\mathcal{N}_{>s} = \frac{4}{3}\pi D_{\rm max}^3 \rho_{\rm cl} \frac{\rm N_{>s}}{\rm N_{samp}} \frac{T_{\rm LISA}}{2\Delta t_{\rm obs}}, \quad (26)$$

where $\rho_{\rm cl}$ is the present-day volume density of young clusters in the local Universe. Equation (26) can be rewritten as (for the assumed $D_{\rm max} = 1500$ Mpc; see Sec. II B)

$$\frac{\mathcal{N}_{>s}}{\rho_{\rm cl}/{\rm Mpc}^{-3}} = 7.069 \frac{\rm N_{>s}}{\rm N_{samp}} \frac{(T_{\rm LISA}/{\rm yr})}{(\Delta t_{\rm obs}/{\rm Gyr})}. \quad (27)$$

Table I shows the $\rm N_{>s}$ and $\mathcal{N}_{>s}/\rho_{\rm cl}$ values for $s = 2$, 5, and 10 for four local Universe samples with Z ranges 0.0001–0.02 and 0.005–0.02 and $T_{\rm LISA} = 5$ yr and 10 yr. Also shown are the intrinsic source counts, $\rm N_0$ and $\mathcal{N}_0/\rho_{\rm cl}$, corresponding to S/N > 0. For each local Universe, $\rm N_{samp} \approx 2.3 \times 10^4$. By taking half of this $\rm N_{samp}$, it is found that all the source counts also become nearly half, implying that such $\rm N_{samp}$ yields statistically convergent counts.

Figure 2 shows the probability distributions (probability density function; hereafter PDF) of the properties of LISA BBH sources at the present cosmic age, that have S/N > 5, as compiled from local Universe samples with Z ranges 0.0001–0.02 (blue-lined histogram) and 0.005–0.02 (red-lined histogram). All the distributions in Fig. 2 correspond to $T_{\rm LISA} = 5$ yr. The top-left panel shows the PDF of the "mean eccentricity" $\bar{e}$ over the detected GW frequency window. $\bar{e}$ represents the most likely eccentricity of the BBH when its GW signal is observed by the detector and is measured, in this study, by the expression

$$\bar{e} = \frac{(2-\kappa_1)e_1 + \kappa_1 e_2}{2}. \quad (28)$$

Here κ_1 is the transience of the GW source as defined in Sec. II B. When $\kappa_1 \to 0$ (the source is nearly invariant over $T_{\rm LISA}$), $\bar{e} \to e_1$, the eccentricity of the binary at the minimum $f_{\rm GWp,z}$ satisfying the visibility conditions. When $\kappa_1 = 1$ (the source is variable over timescales $\lesssim T_{\rm LISA}$), $\bar{e} = (e_1 + e_2)/2$, midway between the eccentricities e_1 and e_2 ($e_1 > e_2$), at the minimum and maximum $f_{\rm GWp,z}$ satisfying the visibility conditions, respectively (see Fig. 1).

The cutoff of the $\bar{e}$ distribution at $\bar{e} = 0.7$ is simply due to the adopted criterion $e \leq 0.7$ for visibility by LISA (Sec. II B). Despite the fact that the BBHs' PN inspirals typically start with a high e, the majority of those with $e \leq 0.7$ are already well circularized within the adopted "bucket" frequency range of $10^{-3} - 10^{-1}$ Hz (see Fig. 10 of Ref. [21]; see also Ref. [19]). This causes the PDF to increase with decreasing $\bar{e}$ (top-left panel of Fig. 2). As is typical for dynamically assembled BBH inspirals [21,58], which is the case for the vast majority of inspirals from the present models, the distribution of the mass ratio, $q \equiv \rm M_2/M_1$ ($\rm M_1 \geq M_2$), of the LISA-visible BBHs is strongly biased towards unity (Fig. 2, top-right panel). However, sources as asymmetric as $q < 0.4$ are possible for a local Universe extending to the most metal-poor environments.

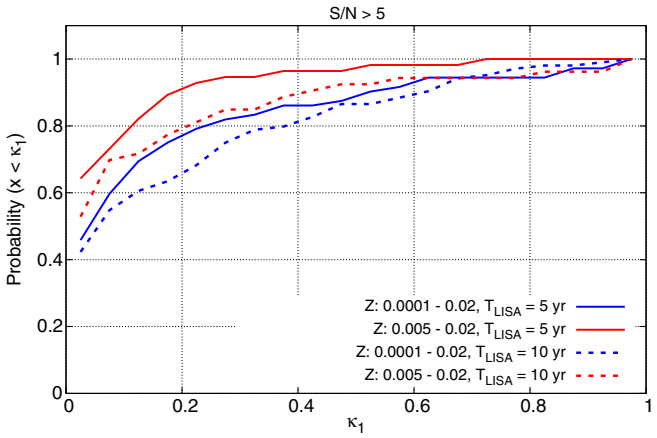

FIG. 3. Cumulative probability distribution of the transience, κ_1 [Eq. (17), Sec. II B], of LISA BBH sources, with S/N > 5, at the present cosmic age from a representative local Universe constructed with the computed model clusters (Sec. II). The distributions are shown for metallicity ranges 0.0001–0.02 and 0.005–0.02, and for $T_{\rm LISA} = 5$ and 10 yr LISA mission lifetimes, as indicated in the legend.

The distribution of the total mass, $M_{\rm tot}$, of the LISA BBH sources is bimodal (Fig. 2, bottom-left panel). The lower mass peak (spanning over 20 $M_\odot$–40 $M_\odot$) is due to the ambience of lower-mass BBH inspirals over the $\lesssim$5 Gyr delay times considered here (Sec. II B); see Fig. 9 of Ref. [21]. The higher mass peak, beyond 60 $M_\odot$, appears since despite the relative rarity of such massive BBH inspirals, they are the brightest GW sources (with the highest $\tilde{h}_c$ and κ). Note that this bimodal feature appears irrespective of the metallicity range of the local Universe. The feature is also mildly present in the PDF of the detector-frame chirp mass, $M_{\rm ch,z}$, of the LISA BBH sources (Fig. 2, bottom-right panel).

Figure 3 shows the cumulative probability distribution of the transience, κ_1 (Sec. II B), of the present-day LISA BBH sources that have S/N > 5, as compiled from the local Universe samples considered here. Shown are the cumulative PDFs for both metallicity ranges, 0.0001–0.02 (blue lines) and 0.005–0.02 (red lines), and for $T_{\rm LISA} = 5$ yr (solid lines) and 10 yr (dashed lines). A LISA source would reach merger—i.e., exit the LISA band and become visible in the LIGO-Virgo band—within twice the LISA mission time if $\kappa_1 \geq 0.5$. According to Fig. 3, with S/N > 5 and $T_{\rm LISA} = 5$ yr, the fraction of BBHs exhibiting such "LISA-LIGO" visibility [8] is $\approx$15% ($\approx$5%) for the $0.0001 \leq Z \leq 0.02$ ($0.005 \leq Z \leq 0.02$) local Universe. With S/N > 5 and $T_{\rm LISA} = 10$ yr, the fraction is $\approx$15% ($\approx$10%) for $0.0001 \leq Z \leq 0.02$ ($0.005 \leq Z \leq 0.02$).

With an estimate of the local volume density of YMCs and OCs, $\rho_{\rm cl}$, the values of $\mathcal{N}_{>s}/\rho_{\rm cl}$ in Table I can be

utilized to estimate the present-day LISA BBH source count. Here a preliminary estimate of $\rho_{\rm cl}$ is used, which is based on the observed local density of GCs of $\rho_{\rm GC} \approx 2.6$ Mpc^{-3} [54,105] (taking $h \equiv H_0/[100\ {\rm km\,s^{-1}}] = 0.674$). Due to the observed power-law birth mass function of clusters with index ≈ -2 [89–92] alone, YMCs and OCs of the mass range considered here ($10^4\ M_\odot$–$10^5\ M_\odot$) would be ≈20 times more numerous than GCs [19], resulting in $\rho_{\rm cl} \approx 52$ Mpc^{-3}. The number of LISA BBH sources for $T_{\rm LISA} = 5$ yr would accordingly be $\mathcal{N}_{>2} \approx 174$, $\mathcal{N}_{>5} \approx 56$, $\mathcal{N}_{>10} \approx 31$ ($\mathcal{N}_{>2} \approx 107$, $\mathcal{N}_{>5} \approx 44$, $\mathcal{N}_{>10} \approx 23$) from the local Universe with $0.0001 \leq Z \leq 0.02$ ($0.005 \leq Z \leq 0.02$). For $T_{\rm LISA} = 10$ yr, $\mathcal{N}_{>2} \approx 483$, $\mathcal{N}_{>5} \approx 164$, $\mathcal{N}_{>10} \approx 71$ ($\mathcal{N}_{>2} \approx 252$, $\mathcal{N}_{>5} \approx 85$, $\mathcal{N}_{>10} \approx 48$) for $0.0001 \leq Z \leq 0.02$ ($0.005 \leq Z \leq 0.02$). For $T_{\rm LISA} = 5$ yr, the intrinsic count for LISA-visible BBHs is $\mathcal{N}_0 \approx 1039$ ($\mathcal{N}_0 \approx 727$) from the local Universe with $0.0001 \leq Z \leq 0.02$ ($0.005 \leq Z \leq 0.02$). For $T_{\rm LISA} = 10$ yr, $\mathcal{N}_0 \approx 2008$ ($\mathcal{N}_0 \approx 1484$) for $0.0001 \leq Z \leq 0.02$ ($0.005 \leq Z \leq 0.02$).

IV. SUMMARY AND DISCUSSIONS

This study, for the first time, attempts to assess the potential contribution of YMCs and OCs, within the local Universe, in assembling stellar-mass BBHs that are detectable by LISA as per the instrument's proposed design. To that end, a suite of state-of-the-art, direct, PN N-body evolutionary model clusters, incorporating up-to-date stellar evolutionary and remnant formation models and observationally consistent structural properties and stellar ingredients [21], is utilized (Sec. II A). The model set allows us to explore the cluster mass range of $10^4\ M_\odot$–$10^5\ M_\odot$ representing the regime where clusters form as YMCs, over the cosmic SFH, and evolve in the long term to become moderately massive, ∼Gyr-old OCs. In this study, model clusters up to ≈5 Gyr age (formation redshift ≤ 0.5) are explored, as is typical for intermediate-aged OCs. The BBH inspirals from them, that would be present at the current cosmic epoch in LISA's most sensitive GW frequency range of $10^{-3} - 10^{-1}$ Hz with eccentricity < 0.7 and exceeding an S/N threshold (Fig. 1), are tracked (Sec. II B). For this purpose, samples of the local Universe, comprising $\sim 10^4$ clusters (Table I) and having a LISA visibility limit of 1500 Mpc, are constructed out of the evolutionary cluster models, following the observed cluster birth mass function and SFH and adopting the standard cosmological framework (Sec. II B). A sample local Universe comprises either the full metallicity range of the cluster models, $0.0001 \leq Z \leq 0.02$ (most of which have $Z \geq 0.001$), implying that the local volume well includes LMC-like or sub-LMC metal-poor environments, or only the $0.005 \leq Z \leq 0.02$ models, implying that the local volume is made predominantly of metal-rich environments (Table I).

A drawback of the present approach is that a cluster's metallicity is completely decoupled from its formation epoch according to the cosmic SFH. However, this is not critical, since only recent formation redshifts of $z_f \leq 0.5$ are considered. How ambient metal-poor environments are in the Local Universe is still largely an open question [93,106]. Rather, the two Z ranges considered here enable exploring the impact of metallicity on LISA source counts and properties. Indeed, the local Universe, including the metal-poor clusters, typically yields larger, by up to a factor of 2, present-day LISA source counts (Table I). This is due to the fact that low-Z clusters yield more massive BBH inspirals (since low-Z stellar progenitors produce more massive BHs [28,43]), so that the present-day LISA BBHs are biased towards higher masses (Fig. 2, bottom panels), which are also generally brighter GW sources. In a forthcoming study, metallicity-dependent SFH (e.g., Refs. [107,108]) will be applied in such an exercise.

For both metallicity regimes, the distribution of total mass, $M_{\rm tot}$, of the present-day LISA BBHs exhibits a bimodal feature (Fig. 2, bottom-left panel; Sec. III). For both cases, the present-day LISA BBH sources are predominantly of similar component masses (mass ratio $q \approx 1$), although dissimilar-mass sources of $q < 0.4$ are possible from the metal-poorer local Universe (Fig. 2, top-right panel). For both types of local Universe, the present-day LISA BBH sources are generally eccentric ($e < 0.7$), although they are biased towards being circular (Fig. 2, top-left panel; Sec. III).

Stellar-mass LISA BBH sources are persistent, with the source properties varying mildly (as given by their transience, κ_1; see Sec. II B) over the LISA mission lifetime, $T_{\rm LISA}$, for the majority of them. However, a small fraction of them would still exhibit significant evolution as they undergo PN inspiral. For the metal-poorer local Universe, ≈15% of the present-day LISA BBHs with S/N > 5 would show up in the LIGO-Virgo frequency band within twice the mission lifetime, and < 5% of the sources would do so within the mission time, for $T_{\rm LISA} = 5$ or 10 yr (Fig. 3; Sec. III). For the metal-richer local Universe, the former fraction is < 10%.

Table I shows the estimated number of present-day LISA BBH sources, $\mathcal{N}_{>s}$, with S/N thresholds $s = 2$, 5, and 10, for both metallicity regimes and for 5 yr and 10 yr mission lifetimes. The entries are scaled with respect to the present-day volume density, $\rho_{\rm cl}$, of YMCs and OCs in the local Universe [see Eq. (27)]. Since such clusters continue to form and evolve with the cosmic evolution of star formation [94], $\rho_{\rm cl}$ depends on the fraction of stars forming in bound clusters and the fraction of such clusters surviving the violent birth environment and conditions [71,73–75,109,110], all of which, and hence $\rho_{\rm cl}$, are poorly constrained to date. By scaling the observed volume density of GCs based on observed cluster mass function, it can be inferred that YMCs and OCs of $\lesssim$5 Gyr age in the metal-poorer local Universe would provide ≈56 (≈164) LISA

BBH sources with S/N > 5, for a 5 yr (10 yr) mission time (Table I; Sec. III). For the metal-richer local Universe, the corresponding source counts are ≈44 (≈85). Therefore, YMCs and OCs would yield LISA-visible BBHs in numbers about an order of magnitude larger than those from GCs [20]. Intrinsically, there would be ≈1000 (700) present-day, LISA-visible BBHs from YMCs and OCs in the metal-poorer (metal-richer) local Universe, for $T_{\rm LISA} =$ 5 yr (Table I; Sec. III). For $T_{\rm LISA} = 10$ yr, the intrinsic counts nearly double.

Note that the above estimates of present-day LISA sources still represent lower limits. The counts can easily be a few factors higher if the borderline between intermediate-aged OCs and GCs is set at a higher mass (currently, it is $10^5\ M_\odot$ [19]). Also, considering clusters formed at higher redshifts would add to both the present-day source counts from a sample local Universe and the present-day local density of YMCs and OCs, which would also lead to a boost of a few factors in the source counts.

LISA BBH sources in young clusters has been addressed also in other recent studies [58,111]. The eccentricity distribution of LISA BBH sources, as obtained here, qualitatively agrees with the trend of the same presented in Ref. [58]. But unlike these authors, the LISA BBH sources here extend to much higher eccentricities, all the way up to 0.7 (Fig. 2, top-left panel). Note, however, that these authors provide the eccentricity distribution corresponding to $f_{\rm K} = 10^{-2}$ Hz, whereas here the most likely eccentricity over 10^{-3} Hz $\leq f_{\rm GWp,z} \leq 10^{-1}$ Hz [Eq. (28)] is considered. Furthermore, in Ref. [58], nearly all inspiraling systems (that merge within a Hubble time) are dynamically ejected from the clusters, whereas here the inspirals take place either inside the clusters or after getting ejected, the former type being dominant [112,113]. Finally, the present work considers clusters of much higher mass (by a few to 100 times) and much longer evolutionary times than those in Ref. [58], yielding BBH inspirals of much broader orbital morphology. The range and the trend of the eccentricity distribution of LISA BBHs obtained here are qualitatively similar to those for in-cluster inspirals from computed GC models [20], which are a few to 10 times more massive than the present models but incorporate similar physics ingredients.

In the near future, this line of study will be extended to incorporate cosmic metallicity evolution and SFH up to high redshifts. The same methodology can be applied to obtain LIGO-Virgo compact binary merger rates from YMCs and OCs, the study of which is underway (see, e.g., Ref. [114] for an alternative approach). The present set of computed model clusters is being extended in mass and density.

ACKNOWLEDGMENTS

S. B. is thankful to the anonymous referee for constructive comments and useful suggestions that have helped to improve the manuscript. S. B. acknowledges the support from the Deutsche Forschungsgemeinschaft (DFG; German Research Foundation) through the individual research grant "The dynamics of stellar-mass black holes in dense stellar systems and their role in gravitational wave generation" (No. BA 4281/6-1; PI: S. Banerjee). This work has benefited from discussions with Sverre Aarseth, Pablo Laguna, Deirdre Shoemaker, Chris Belczynski, Harald Pfeiffer, Philipp Podsiadlowski, Pau Amaro-Seoane, Xian Chen, Elisa Bortolas, and Rainer Spurzem. S. B. acknowledges the generous support and efficient system maintenance of the computing teams at the AIfA and the HISKP. S. B. acknowledges the hospitality and the energetic discussions during the Tal Alexander Meeting 2019 (held at the posadas de Alájar and San Marcos in Alájar, Spain during August 25–September 4, 2019) which have motivated this work.

[1] M. Armano, H. Audley, G. Auger, J. T. Baird, M. Bassan, P. Binetruy, M. Born, D. Bortoluzzi *et al.*, Phys. Rev. Lett. **116**, 231101 (2016).
[2] P. Amaro-Seoane, H. Audley, S. Babak, J. Baker, E. Barausse, P. Bender, E. Berti, P. Binetruy *et al.*, arXiv:1702.00786.
[3] J. Abadie, B. P. Abbott, R. Abbott, M. Abernathy, T. Accadia, F. Acernese, C. Adams, R. Adhikari, P. Ajith, B. Allen *et al.*, Classical Quantum Gravity **27**, 173001 (2010).
[4] B. P. Abbott, R. Abbott, T. D. Abbott, M. R. Abernathy, F. Acernese, K. Ackley, C. Adams, T. Adams, P. Addesso, R. X. Adhikari *et al.*, Phys. Rev. Lett. **116**, 061102 (2016).
[5] P. Amaro-Seoane, J. R. Gair, M. Freitag, M. C. Miller, I. Mandel, C. J. Cutler, and S. Babak, Classical Quantum Gravity **24**, R113 (2007).
[6] A. J. Ruiter, K. Belczynski, M. Benacquista, S. L. Larson, and G. Williams, Astrophys. J. **717**, 1006 (2010).
[7] K. Holley-Bockelmann and F. M. Khan, Astrophys. J. **810**, 139 (2015).
[8] A. Sesana, Phys. Rev. Lett. **116**, 231102 (2016).
[9] B. P. Abbott, R. Abbott, T. D. Abbott, S. Abraham, F. Acernese, K. Ackley, C. Adams, R. X. Adhikari, V. B. Adya, C. Affeldt *et al.*, Phys. Rev. X **9**, 031040 (2019).
[10] B. P. Abbott, R. Abbott, T. D. Abbott, S. Abraham, F. Acernese, K. Ackley, C. Adams, R. X. Adhikari *et al.*, Astrophys. J. Lett. **892**, L3 (2020).

[11] LIGO Scientific and Virgo Collaborations, Phys. Rev. D **102**, 043015 (2020).
[12] M. J. Benacquista and J. M. B. Downing, Living Rev. Relativity **16**, 4 (2013).
[13] S. Kawamura, M. Ando, T. Nakamura, K. Tsubono, T. Tanaka, I. Funaki, N. Seto, K. Numata *et al.*, J. Phys. Conf. Ser. **122**, 012006 (2008).
[14] M. Arca Sedda *et al.*, arXiv:1908.11375.
[15] J. Luo, L.-S. Chen, H.-Z. Duan, Y.-G. Gong, S. Hu, J. Ji, Q. Liu, J. Mei *et al.*, Classical Quantum Gravity **33**, 035010 (2016).
[16] S. Liu, Y.-M. Hu, J.-d. Zhang, and J. Mei, Phys. Rev. D **101**, 103027 (2020).
[17] A. Nishizawa, E. Berti, A. Klein, and A. Sesana, Phys. Rev. D **94**, 064020 (2016).
[18] A. Nishizawa, A. Sesana, E. Berti, and A. Klein, Mon. Not. R. Astron. Soc. **465**, 4375 (2017).
[19] S. Banerjee, Mon. Not. R. Astron. Soc. **473**, 909 (2018).
[20] K. Kremer, C. L. Rodriguez, P. Amaro-Seoane, K. Breivik, S. Chatterjee, M. L. Katz, S. L. Larson, F. A. Rasio, J. Samsing, C. S. Ye, and M. Zevin, Phys. Rev. D **99**, 063003 (2019).
[21] S. Banerjee, arXiv:2004.07382 [Mon. Not. R. Astron. Soc. (to be published)].
[22] N. Ivanova, S. Justham, X. Chen, O. De Marco, C. L. Fryer, E. Gaburov, H. Ge, E. Glebbeek, Z. Han, X. D. Li, G. Lu, T. Marsh, P. Podsiadlowski, A. Potter, N. Soker, R. Taam, T. M. Tauris, E. P. J. van den Heuvel, and R. F. Webbink, Aston. Astrophys. Rev. **21**, 59 (2013).
[23] K. Belczynski, D. E. Holz, T. Bulik, and R. O'Shaughnessy, Nature (London) **534**, 512 (2016).
[24] I. Mandel and A. Farmer, Nature (London) **547**, 284 (2017).
[25] S. Stevenson, A. Vigna-Gómez, I. Mandel, J. W. Barrett, C. J. Neijssel, D. Perkins, and S. E. de Mink, Nat. Commun. **8**, 14906 (2017).
[26] N. Giacobbo, M. Mapelli, and M. Spera, Mon. Not. R. Astron. Soc. **474**, 2959 (2018).
[27] V. Baibhav, E. Berti, D. Gerosa, M. Mapelli, N. Giacobbo, Y. Bouffanais, and U. N. Di Carlo, Phys. Rev. D **100**, 064060 (2019).
[28] S. Banerjee, K. Belczynski, C. L. Fryer, P. Berczik, J. R. Hurley, R. Spurzem, and L. Wang, Astron. Astrophys. **639**, A41 (2020).
[29] G. M. Fuller, A. Kusenko, I. Mocioiu, and S. Pascoli, Phys. Rev. D **68**, 103002 (2003).
[30] C. L. Fryer and A. Kusenko, Astrophys. J. Suppl. Ser. **163**, 335 (2006).
[31] J. Samsing and D. J. D'Orazio, Mon. Not. R. Astron. Soc. **481**, 5445 (2018).
[32] B.-M. Hoang, S. Naoz, B. Kocsis, W. M. Farr, and J. McIver, Astrophys. J. Lett. **875**, L31 (2019).
[33] H. C. Plummer, Mon. Not. R. Astron. Soc. **71**, 460 (1911).
[34] L. Spitzer, *Dynamical Evolution of Globular Clusters* (Princeton University Press, Princeton, NJ, 1987), p. 191.
[35] D. Heggie and P. Hut, *The Gravitational Million-Body Problem: A Multidisciplinary Approach to Star Cluster Dynamics* (Cambridge University Press, Cambridge, 2003).
[36] H. Sana and C. J. Evans, in *Active OB Stars: Structure, Evolution, Mass Loss, and Critical Limits*, edited by C. Neiner, G. Wade, G. Meynet, and G. Peters, IAU Symposium, Vol. 272 (Cambridge University Press, Cambridge, 2011), pp. 474–485.
[37] M. Moe and R. Di Stefano, Astrophys. J. Suppl. Ser. **230**, 15 (2017).
[38] S. J. Aarseth, *Gravitational N-Body Simulations*, edited by Sverre J. Aarseth (Cambridge University Press, Cambridge, England, 2003).
[39] S. J. Aarseth, Mon. Not. R. Astron. Soc. **422**, 841 (2012).
[40] K. Nitadori and S. J. Aarseth, Mon. Not. R. Astron. Soc. **424**, 545 (2012).
[41] J. R. Hurley, O. R. Pols, and C. A. Tout, Mon. Not. R. Astron. Soc. **315**, 543 (2000).
[42] J. R. Hurley, C. A. Tout, and O. R. Pols, Mon. Not. R. Astron. Soc. **329**, 897 (2002).
[43] K. Belczynski, T. Bulik, C. L. Fryer, A. Ruiter, F. Valsecchi, J. S. Vink, and J. R. Hurley, Astrophys. J. **714**, 1217 (2010).
[44] C. L. Fryer, K. Belczynski, G. Wiktorowicz, M. Dominik, V. Kalogera, and D. E. Holz, Astrophys. J. **749**, 91 (2012).
[45] K. Belczynski, A. Heger, W. Gladysz, A. J. Ruiter, S. Woosley, G. Wiktorowicz, H.-Y. Chen, T. Bulik, R. O'Shaughnessy, D. E. Holz, C. L. Fryer, and E. Berti, Astron. Astrophys. **594**, A97 (2016).
[46] G. Hobbs, D. R. Lorimer, A. G. Lyne, and M. Kramer, Mon. Not. R. Astron. Soc. **360**, 974 (2005).
[47] K. Belczynski, V. Kalogera, F. A. Rasio, R. E. Taam, A. Zezas, T. Bulik, T. J. Maccarone, and N. Ivanova, Astrophys. J. Suppl. Ser. **174**, 223 (2008).
[48] S. Mikkola and K. Tanikawa, Mon. Not. R. Astron. Soc. **310**, 745 (1999).
[49] S. Mikkola and D. Merritt, Astron. J. **135**, 2398 (2008).
[50] Y. Kozai, Astron. J. **67**, 591 (1962).
[51] Y. Lithwick and S. Naoz, Astrophys. J. **742**, 94 (2011).
[52] B. Katz, S. Dong, and R. Malhotra, Phys. Rev. Lett. **107**, 181101 (2011).
[53] F. Antonini, S. Chatterjee, C. L. Rodriguez, M. Morscher, B. Pattabiraman, V. Kalogera, and F. A. Rasio, Astrophys. J. **816**, 65 (2016).
[54] S. F. Portegies Zwart and S. L. W. McMillan, Astrophys. J. Lett. **528**, L17 (2000).
[55] S. Banerjee, H. Baumgardt, and P. Kroupa, Mon. Not. R. Astron. Soc. **402**, 371 (2010).
[56] C. L. Rodriguez, M. Morscher, B. Pattabiraman, S. Chatterjee, C.-J. Haster, and F. A. Rasio, Phys. Rev. Lett. **115**, 051101 (2015).
[57] J. Kumamoto, M. S. Fujii, and A. Tanikawa, Mon. Not. R. Astron. Soc. **486**, 3942 (2019).
[58] U. N. Di Carlo, N. Giacobbo, M. Mapelli, M. Pasquato, M. Spera, L. Wang, and F. Haardt, Mon. Not. R. Astron. Soc. **487**, 2947 (2019).
[59] P. C. Peters, Phys. Rev. **136**, B1224 (1964).
[60] X. Chen and P. Amaro-Seoane, Astrophys. J. Lett. **842**, L2 (2017).
[61] K. Belczynski, J. Klencki, C. E. Fields, A. Olejak, E. Berti, G. Meynet, C. L. Fryer, D. E. Holz *et al.*, Astron. Astrophys. **636**, A104 (2020).

[62] J. G. Baker, W. D. Boggs, J. Centrella, B. J. Kelly, S. T. McWilliams, M. C. Miller, and J. R. van Meter, Astrophys. J. Lett. **682**, L29 (2008).

[63] L. Rezzolla, E. Barausse, E. N. Dorband, D. Pollney, C. Reisswig, J. Seiler, and S. Husa, Phys. Rev. D **78**, 044002 (2008).

[64] J. R. van Meter, M. C. Miller, J. G. Baker, W. D. Boggs, and B. J. Kelly, Astrophys. J. **719**, 1427 (2010).

[65] D. Gerosa and E. Berti, Phys. Rev. D **95**, 124046 (2017).

[66] C. L. Rodriguez, P. Amaro-Seoane, S. Chatterjee, and F. A. Rasio, Phys. Rev. Lett. **120**, 151101 (2018).

[67] M. Morscher, B. Pattabiraman, C. Rodriguez, F. A. Rasio, and S. Umbreit, Astrophys. J. **800**, 9 (2015).

[68] M. Hénon, in *Dynamics of the Solar Systems*, edited by A. Hayli, IAU Symposium, Vol. 69 (D. Reidel Pub. Co., Dordrecht, 1975), p. 133.

[69] P. G. Breen and D. C. Heggie, Mon. Not. R. Astron. Soc. **432**, 2779 (2013).

[70] F. Antonini and M. Gieles, Mon. Not. R. Astron. Soc. **492**, 2936 (2020).

[71] S. N. Longmore, J. M. D. Kruijssen, N. Bastian, J. Bally, J. Rathborne, L. Testi, A. Stolte, J. Dale, E. Bressert, and J. Alves, *Protostars and Planets VI* (University of Arizona Press, Tucson, 2014), p. 291.

[72] E. D. Feigelson, Multiwavelength studies of Young OB Associations, in *The Birth of Star Clusters*, edited by S. Stahler, Astrophysics and Space Science Library, Vol. 424 (Springer International Publishing AG, Cham, 2018), p. 119.

[73] S. Banerjee and P. Kroupa, Formation of very young massive clusters and implications for globular clusters, in *The Birth of Star Clusters*, edited by S. Stahler, Astrophysics and Space Science Library, Vol. 424 (Springer International Publishing AG, Cham, 2018) p. 143.

[74] M. Marks and P. Kroupa, Astron. Astrophys. **543**, A8 (2012).

[75] M. Marks, P. Kroupa, J. Dabringhausen, and M. S. Pawlowski, Mon. Not. R. Astron. Soc. **422**, 2246 (2012).

[76] S. Banerjee and P. Kroupa, Mon. Not. R. Astron. Soc. **447**, 728 (2015).

[77] N. Brinkmann, S. Banerjee, B. Motwani, and P. Kroupa, Astron. Astrophys. **600**, A49 (2017).

[78] B. Shukirgaliyev, G. Parmentier, P. Berczik, and A. Just, Astron. Astrophys. **605**, A119 (2017).

[79] M. Spera, M. Mapelli, N. Giacobbo, A. A. Trani, A. Bressan, and G. Costa, Mon. Not. R. Astron. Soc. **485**, 889 (2019).

[80] S. Chatterjee, C. L. Rodriguez, and F. A. Rasio, Astrophys. J. **834**, 68 (2017).

[81] K. Kremer, S. Chatterjee, C. L. Rodriguez, and F. A. Rasio, Astrophys. J. **852**, 29 (2018).

[82] S. Banerjee, Mon. Not. R. Astron. Soc. **481**, 5123 (2018).

[83] A. Burrows and J. Hayes, Phys. Rev. Lett. **76**, 352 (1996).

[84] C. L. Fryer, Astrophys. J. **601**, L175 (2004).

[85] C. A. Meakin and D. Arnett, Astrophys. J. Lett. **637**, L53 (2006).

[86] C. A. Meakin and D. Arnett, Astrophys. J. **665**, 690 (2007).

[87] K. Kremer, C. S. Ye, N. Z. Rui, N. C. Weatherford, S. Chatterjee, G. Fragione, C. L. Rodriguez, M. Spera, and F. A. Rasio, Astrophys. J. Suppl. Ser. **247**, 48 (2020).

[88] S. F. Portegies Zwart, S. L. W. McMillan, and M. Gieles, Annu. Rev. Astron. Astrophys. **48**, 431 (2010).

[89] C. J. Lada and E. A. Lada, Annu. Rev. Astron. Astrophys. **41**, 57 (2003).

[90] M. Gieles, S. S. Larsen, R. A. Scheepmaker, N. Bastian, M. R. Haas, and H. J. G. L. M. Lamers, Astron. Astrophys. **446**, L9 (2006).

[91] M. Gieles, S. S. Larsen, N. Bastian, and I. T. Stein, Astron. Astrophys. **450**, 129 (2006).

[92] S. S. Larsen, Astron. Astrophys. **494**, 539 (2009).

[93] T. Hsyu, R. J. Cooke, J. X. Prochaska, and M. Bolte, Astrophys. J. **863**, 134 (2018).

[94] P. Madau and M. Dickinson, Annu. Rev. Astron. Astrophys. **52**, 415 (2014).

[95] L. Wen, Astrophys. J. **598**, 419 (2003).

[96] P. C. Peters and J. Mathews, Phys. Rev. **131**, 435 (1963).

[97] L. Barack and C. Cutler, Phys. Rev. D **70**, 122002 (2004).

[98] W. H. Press, S. A. Teukolsky, W. T. Vetterling, and B. P. Flannery, *Numerical Recipes in FORTRAN. The Art of Scientific Computing* (Press Syndicate of the University of Cambridge, Cambridge, New York, Melbourne, 1992).

[99] T. Robson, N. J. Cornish, and C. Liu, Classical Quantum Gravity **36**, 105011 (2019).

[100] A. Sesana, F. Haardt, P. Madau, and M. Volonteri, Classical Quantum Gravity **22**, S363 (2005).

[101] B. Willems, V. Kalogera, A. Vecchio, N. Ivanova, F. A. Rasio, J. M. Fregeau, and K. Belczynski, Astrophys. J. **665**, L59 (2007).

[102] R. M. O'Leary, B. Kocsis, and A. Loeb, Mon. Not. R. Astron. Soc. **395**, 2127 (2009).

[103] E. L. Wright, Publ. Astron. Soc. Pac. **118**, 1711 (2006).

[104] N. Aghanim, Y. Akrami, M. Ashdown, J. Aumont, C. Baccigalupi, M. Ballardini, A. J. Banday, R. B. Barreiro *et al.* (Planck Collaboration), Astron. Astrophys. **641**, A6 (2020).

[105] S. van den Bergh, Astron. J. **110**, 2700 (1995).

[106] Y. I. Izotov, T. X. Thuan, N. G. Guseva, and S. E. Liss, Mon. Not. R. Astron. Soc. **473**, 1956 (2018).

[107] P. Madau and T. Fragos, Astrophys. J. **840**, 39 (2017).

[108] M. Chruslinska and G. Nelemans, Mon. Not. R. Astron. Soc. **488**, 5300 (2019).

[109] M. R. Krumholz, M. R. Bate, H. G. Arce, J. E. Dale, R. Gutermuth, R. I. Klein, Z. Y. Li, F. Nakamura, and Q. Zhang, in *Protostars and Planets VI*, edited by H. Beuther, R. S. Klessen, C. P. Dullemond, and T. Henning (University of Arizona Press, Tucson, 2014), p. 243.

[110] F. Renaud, New Astron. Rev. **81**, 1 (2018).

[111] S. Rastello, P. Amaro-Seoane, M. Arca-Sedda, R. Capuzzo-Dolcetta, G. Fragione, and I. Tosta e Melo, Mon. Not. R. Astron. Soc. **483**, 1233 (2019).

[112] S. Banerjee, Mon. Not. R. Astron. Soc. **467**, 524 (2017).

[113] O. Anagnostou, M. Trenti, and A. Melatos, arXiv: 2009.00178.

[114] F. Santoliquido, M. Mapelli, Y. Bouffanais, N. Giacobbo, U. N. Di Carlo, S. Rastello, M. C. Artale, and A. Ballone, Astrophys. J. **898**, 152 (2020).